Materials Chemistry and Physics 269 (2021) 124735

Contents lists available at ScienceDirect

Materials Chemistry and Physics

journal homepage: www.elsevier.com/locate/matchemphys

Molybdenum trioxide embedded graphitic carbon nitride sheets modified electrode for caffeine sensing in green tea and coffee powder

Gopal Boopathy [a], Murugan Keerthi [c], Shen-Ming Chen [c,**], S. Meenakshi [b,*], M.J. Umapathy [a]

[a] Department of Chemistry, College of Engineering, Guindy, Anna University, Chennai, 600 025, Tamil Nadu, India
[b] Department of Chemistry, School of Basic Sciences, Vels Institute of Science, Technology and Advanced Studies (VISTAS), Pallavaram, Chennai, 600 117, Tamil Nadu, India
[c] Department of Chemical Engineering and Biotechnology, National Taipei University of Technology, No.1, Section 3, Chung-Hsiao East Road, Taipei, 106, Taiwan

HIGHLIGHTS

- New approach for electrochemical sensing of caffeine based MoO_3 grown on the GCNS modified SPCE.
- The lowest LOD and sensitivity are calculated to be 21.24 nM and 11.584 μA $\mu M^{-1}cm^{-2}$ for CAF sensing.
- The proposed electrode was successfully applied for the detection of CAF in green tea and coffee powder samples.

ARTICLE INFO

Keywords:
Caffeine
Psychomotor stimulant drug
Graphitic carbon nitride sheets
MoO_3 particles
Green tea

ABSTRACT

The development of a screen-printed electrochemical sensor based on molybdenum trioxide (MoO_3) grown on the graphitic carbon nitride sheets (GCNS) nanocomposite was investigated for its ability to serve as an extremely sensitive and selective sensor towards caffeine (CAF). The MoO_3@GCNS nanocomposite was synthesized through a simple hydrothermal method and was analyzed using spectroscopic and microscopic techniques (XPS, FT-IR, and FE-SEM). Voltammetry outcomes illustrated the enhancement of electrocatalytic oxidation of CAF at MoO_3@GCNS modified electrode with higher oxidation current and also significantly reduced oxidation potential because of the synergetic effect between MoO_3 and GCNS as compared to pure MoO_3 and GCNS modified electrode. DPV results of MoO_3@GCNS modified electrode displayed two wide straight lines (ranges of 0.5–359 μM and 410–810 μM) with a limit of detection of 21.24 nM with appreciable selectivity of 11.584 μA $\mu M^{-1}cm^{-2}$ for CAF sensing. The modified electrode was further used for the detection of CAF in green tea and coffee powder samples.

1. Introduction

Refreshing beverages (coffee and green tea) are most common in the globe for the reason that it has an excellent flavor and health benefits. The presence of active components in these beverages is providing good health benefits. One of the main active components existing in tea and coffee is caffeine [1,2]. The active alkaloid component of caffeine (CAF) (1, 3, 7-trimethylxanthine) plays an important role in human being such as stimulates the CNS, secretion of gastric acid, diuresis, increases blood pressure [3,4], etc. CAF is involved in the preparation of drugs used for various treatments like difficulty in breathing, stuffy nose, pain in the head, increasing general fitness [5], etc. Intake of CAF content more than recommended doses (150–200 mg/kg of body weight) causes health problems and this condition persists causing death, especially for younger patients such as infants and toddlers [6,7]. So the accurate level of CAF detection is very important. The various methods have been explored for CAF detection, such as HPLC [8], spectrophotometry [9], capillary electrophoresis (CE) [10], chromatography [11], and microfluidic device [12]. Among this method, electrochemical techniques are rapid, inexpensive, the wide straight line ranges with higher sensitivity, suitable for real sample analysis with good accuracy.

Graphitic carbon nitride (GCN) has accomplished great growing interest in developing new electrocatalyst due to its unique electronic structure by 2D planes of the tris-triazine unit and pi conjugation in the

* Corresponding author.
** Corresponding author.
E-mail addresses: smchen1957@gmail.com, smchen78@ms15.hinet.net (S.-M. Chen), meenakshivanitha@gmail.com (S. Meenakshi).

https://doi.org/10.1016/j.matchemphys.2021.124735
Received 12 October 2020; Received in revised form 6 May 2021; Accepted 9 May 2021
Available online 26 May 2021

middle of GCN composite [13,14]. It has been demonstrated good photo and electrocatalytic activities in various fields like electrolysis of water, battery storage, organocatalyst, monitoring environmental pollutants [15], etc. Moreover, carbon nitride sheets are eco-friendly, economically cheap, and excellent light absorption characteristics [16], which has a hybrid electronic structure is one of the promising material for the electrochemical sensor [17]. There are plenty of GCN based electrocatalysts that have been investigated. Moreover, many researchers have been done significant efforts to improve the electrochemical performance of GCN by coupling it into other metal oxides, metal nanoparticles, and carbon materials. For Example, Jing et al., developed an ultrasensitive electrochemical sensor based on GCN/CuO nanocomposites for dopamine detection [15], and Yi et al., demonstrated NiO and Co_3O_4 co-doped GCN nanocomposites with excellent photoelectrochemical properties under visible light for detection of tetrabromobisphenol-A with LOD of 0.1 mmol L^{-1} [18]. In this view, the efficient electrocatalyst developed by modifying the electronic structure of GCN with an appropriate nanosized metal oxide. Meanwhile, GCN act as a good substrate to develop hetero-structured electrochemical sensing materials due to its providing anchoring sites to attach and enriched electrocatalytic activity [19]. Molybdenum trioxide (MoO_3) has generally used as an electrocatalyst due to its higher electrical conductivity and stability [20,21]. The MoO_3 is extensively studied in various applications such as gas sensors, supercapacitors, solar-energy absorbers, rechargeable lithium-ion batteries, and electrochemical sensor materials [22,23]. The electrochemical performance is enhanced by altering the inter junction interface of electrochemical nanomaterials by doping the suitable catalyst. Due to the excellent inherent catalytic activity, MoO_3 has been also used to modify the GCN electronic structure and enhance the electrocatalytic activity. In this study, the electrocatalytic activity of GCNS altered with MoO_3. Due to the 60% abundance of N aromatic content in the GCN, providing its lone pair of electrons to Mo metal ions during the synthesis process resulting in the formation coordination covalent bond [24,25]. The electron-rich MoO_3@GCNS nanocomposite acts as an electron donor, where GCN transfers its electron to the analyte molecule. This stable MoO_3@GCNS nanocomposite is expected to act as a favorable catalyst for the electrochemical oxidation of CAF in green tea and coffee samples.

2. Experimental section

2.1. Materials and instrumentations

Melamine, ammonium molybdate tetrahydrate [$(NH_4)_6Mo_7O_{24}{\cdot}4H_2O$], caffeine, and all the required chemicals were received from Biocorporals, Chennai. Supporting electrolyte (0.1 M PBS) prepared using the mixture Na_2HPO_4 and NaH_2PO_4. The chemical and valence state of the elements investigated through XPS results using a Thermo ESCALAB 250 instrument. Functional groups, crystalline structure, morphological characterization, and electrochemical measurements of the prepared material investigated from FT-IR spectroscopy (Perkin-Elmer IR spectrometer), Powder X-ray diffractometer (Cu Kα radiation is k = 1.54 Å, XPERT-PRO, Netherland), Hitachi S-3000H (FE-SEM, Japan) and cyclic voltammetry (CHI, USA). In the voltammetry technique, a three-electrode cell system having a screen-printed carbon electrode (SPCE) (working electrode), platinum wire (counter electrode), and Ag/AgCl (reference electrode). All the experiments were performed triplicate. The stock solutions of CAF (0.1 M) were prepared freshly with DD water and stored in a refrigerator at 4 °C. The pH of the solution was checked by using Elico-pH meter. The MoO_3@GCNS modified electrode was detected using cyclic voltammetry (Potential window: 0.8 V to + 1.6 V, Scan rate: 50 $mV.s^{-1}$), differential pulse voltammetry (Pulse width: 50 mV, Pulse amplitude: 25 mV).

2.2. Preparation of GCN sheets

The GCNS was synthesized using melamine reported by previous literature [13]. A ceramic alumina boat contains 3 g of melamine was placed in a muffle furnace with a temperature of around 550 °C for 4 h. After cooled down to room temperature, the yellow powder of GCN was washed with double distilled (DD) water to remove un-exfoliated GCNS and dried in an oven at 60 °C.

2.3. Preparation of MoO_3@GCNS

The MoO_3 powder was prepared by a solid-state decomposition method. The ammonium molybdate tetrahydrate was heated at 500 °C for 4 h. After that, the obtained powder was washed with DD water and dried in an oven at 60 °C for 6 h [26]. To prepare MoO_3@GCNS nanocomposite, 10 mg GCNS and MoO_3 were mixed with DD water and stirred for 15 min using a magnetic stirrer followed by ultra-sonicated for 30 min to obtain a homogeneous mixture by self-assembly between the MoO_3 and GCNS by through strong interaction, thus yielding stable MoO_3@GCNS nanocomposite.

2.4. Fabrication of MoO_3@GCNS modified electrode

To prepare the MoO_3@GCNS modified electrode, 2 mg of the synthesized MoO_3@GCNS powder was dispersed in 1 mL of DD water via ultrasonic treatment for 20 min. Then, 6.0 μL of MoO_3@GCNS slurry was dropped on the surface of SPCE with a micropipette and then dried at room temperature. For control studies, MoO_3 and GCNS modified SPCE was prepared by the same process.

3. Results and discussion

3.1. Characterization of MoO_3@GCNS

Surface elemental composition and chemical states of MoO_3@GCNS nanocomposite were studied using the XPS technique. The survey spectrum of MoO_3@GCNS (Fig. 1A), showed that the presence of elements such as C, N, Mo, and O in the MoO_3@GCNS, which may be due to the MoO_3 embedded into GCNS. Fig. 1B shows the XPS spectra of C 1s, which exhibits three peaks at 285 eV, 288 eV, and 289 eV due to graphite-like sp^2 C═C, s-triazine unit, and N trigonally bonded to three sp^2 C-atoms (N $(C)_3$ groups) respectively [27]. The N1s spectra of GCNS were divided into three typical peaks at 398.7, 399.2, and 401.2 eV (Fig. 1C), which were attributed to C–N═C, C–N, and C–N–H bond, respectively. For MoO_3@GCNS, these three peaks shifted to lower energy at 398.2, 398.7, and 400.2 eV compared with GCNS indicated the interaction between GCNS and MoO_3 [14,28]. The Mo $3d_{5/2}$ and Mo $3d_{3/2}$ orbital spin splitting have occurred at 235.4 eV and 238.5 eV corresponding to the Mo^{6+} cations present in MoO_3. Besides, the two small bands observed at 231.9 eV ($3d_{5/2}$) and 233 eV ($3d_{5/2}$) ascribed to Mo^{4+} and Mo^{5+} connected with oxygen-vacancies of MoO_3 as shown in Fig. 1D [29]. The O 1s XPS spectrum shows (Fig. 1E), the peak at 532.85 eV, which corresponds to the lattice oxygen present in MoO_3 which results further confirmed that the formation of MoO_3@GCNS composite [30].

Fig. 1F shows the FT-IR spectrum of the GCNS, MoO_3, and MoO_3@GCNS. In the spectrum of MoO_3@GCNS, the characteristics peaks of both GCNS and MoO_3 were observed. In the spectrum of GCNS, peak positioned at 1290, 1402, 1465, 1541, and 1625 cm^{-1} is assigned to stretching vibration of C–N, and the peak at 808 cm^{-1} due to N–C═N units in GCNS structure [31]. The characteristic MoO_3 peak at 591 and 876 cm^{-1} owing to the MoO_3 and Mo–O–Mo units, whereas the band at 992 cm^{-1} attributed to the stretching mode Mo═O which confirming that MoO_3 strongly incorporated with GCNS [26]. This is confirmed from the spectrum of pure MoO_3 and GCNS.

The crystalline natures of the synthesized GCNS and MoO_3@GCNS

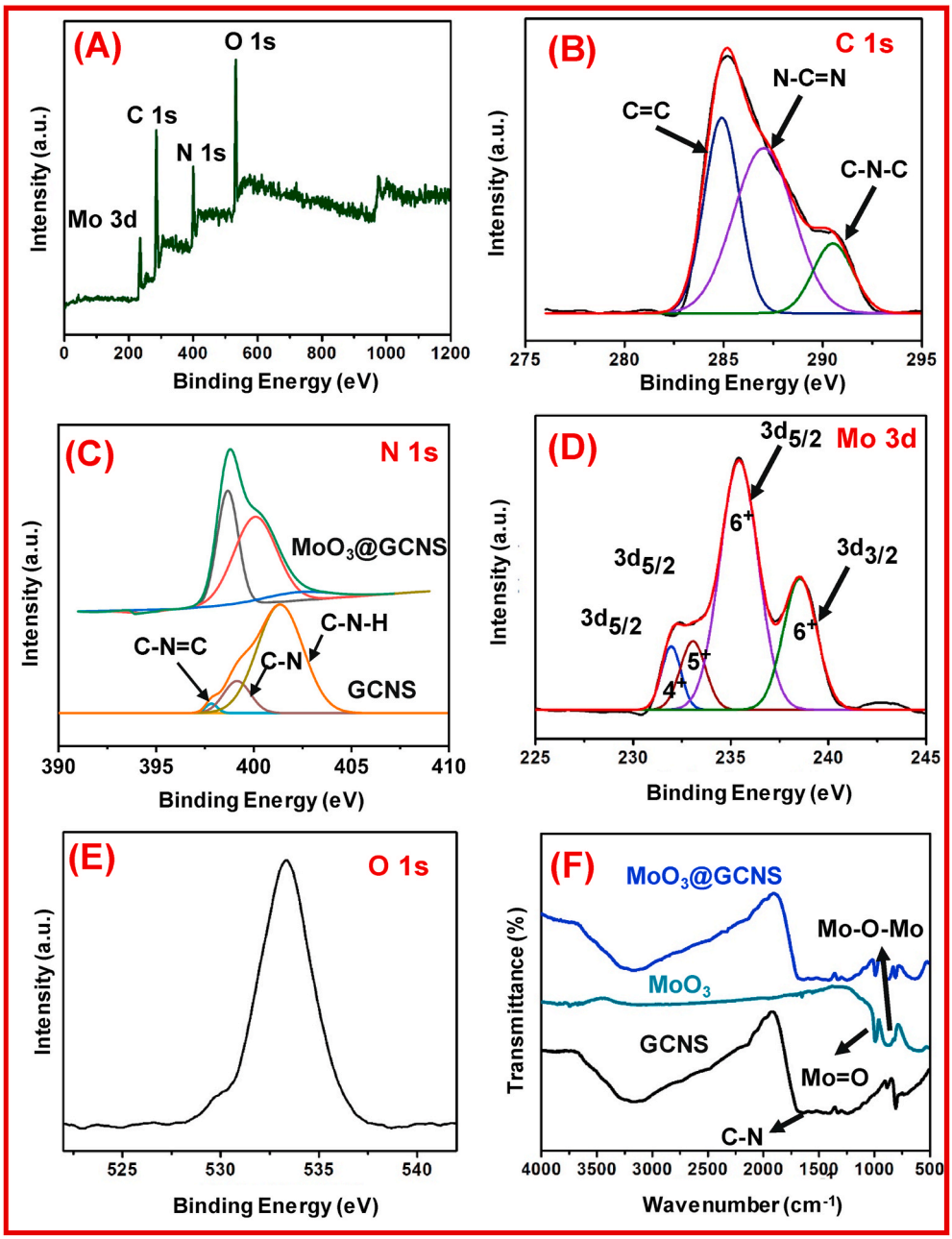

Fig. 1. XPS spectrum of the MoO_3@GCNS (A) Survey spectrum (B) C 1s, (C) N 1s, (D) Mo 3d, (E) O 1s, and (F) FT-IR spectrum of MoO_3@GCNS.

were investigated using XRD (Fig. 2A). XRD pattern of GCNS exhibits the diffraction peak at 24.34° corresponding to (002) plane reflects the typical interlayer piling of the structural aromatic ring and the peak at 18° corresponding to (100) plane assigned to the inter-planar structural packing (JCPDS 87-1526) [14]. Moreover, typical peaks of GCNS and MoO_3 have appeared in the nanocomposite. Besides the main characteristics peaks of MoO_3 at 12.8°, 23.12°, 25.7°, 25.38°, 27.3°, and 39.0°, connecting to the planes of (020), (110), (040), (120), (021), and (060) [JCPDF 35-0609] [26]. Fig. 2B and C displays the FE-SEM image of pure GCN powder and MoO_3 particles. It can be seen that MoO_3 crystalline shows clear edges and a wider particle size distribution. The MoO_3@GCNS nanocomposite visibly detected GCNS wrapped around the MoO_3 particles (Fig. 2D). The EDX spectrum and corresponding mapping images of MoO_3@GCNS nanocomposite indicated that the presence of C, N, Mo, and O with a weight percentage of 60.86, 30.22, 4.14, and 4.78 respectively which confirms the GCNS wrapped around the MoO_3 particles (Fig. 3A–F).

3.2. Electrochemical behavior of MoO_3@GCNS

Electrochemical behavior of SPCE, MoO_3, GCNS, MoO_3@GCNS modified electrode were investigated using 5 mM $K_3[Fe(CN)_6]^{3-/4-}$ with 0.1 M KCl solution by voltammetry technique (Fig. 4A). The electrodes revealed redox peaks in the presence of 5 mM $K_3[Fe(CN)_6]^{3-/4-}$ with 0.1 M KCl solution. As compared to other electrodes, the MoO_3@GCNS electrode displays a sharp peak current response with lower peak potential separation (ΔE_p = 84 mV), and the ΔE_p values of other electrodes such as SPCE, MoO_3, and GCNS modified electrode were shown as 151 mV, 111 mV, and 102 mV which indicated that the excellent electrocatalytic activity and fast electron transfer kinetics of the MoO_3@GCNS/SPCE. Furthermore, the anodic and cathodic peak response ratio is 1.14 at MoO_3@GCNS/SPCE indicating an excellent reversible redox reaction. The electroactive surface area was calculated using Randles–Sevcik equation at different sweep rates from 20 to 300 mVs^{-1} (Fig. 4B).

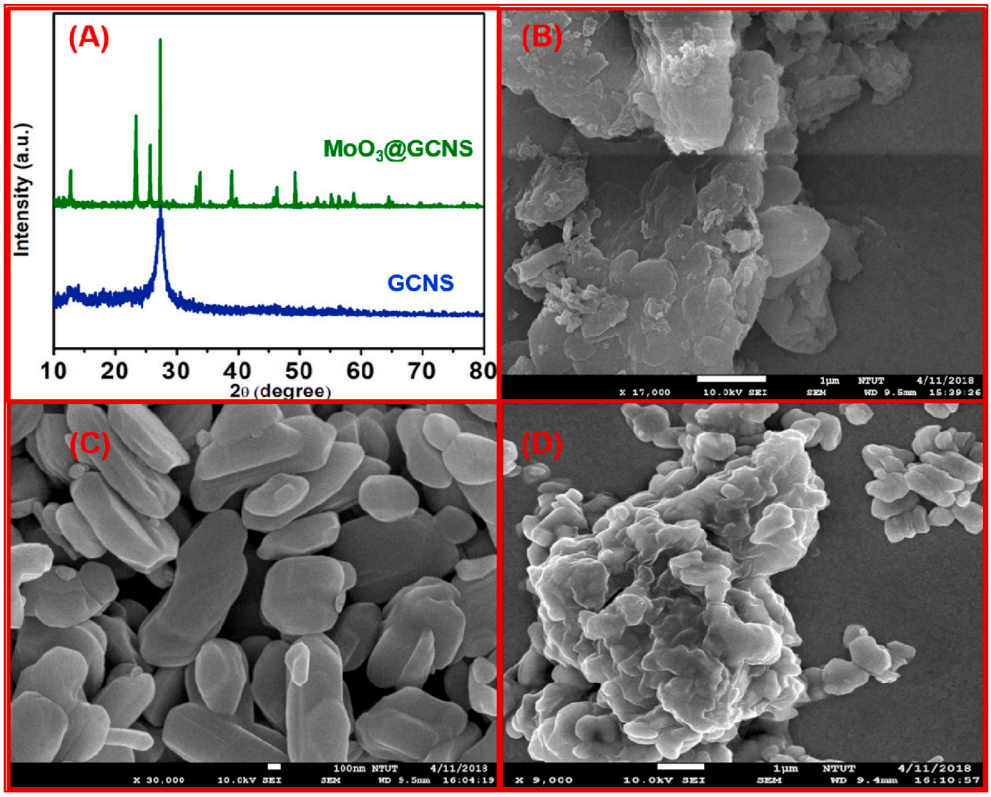

Fig. 2. (A) XRD pattern, (B) FE-SEM images of the pristine GCN, (C) MoO_3, and (D) MoO_3@GCNS nanocomposite.

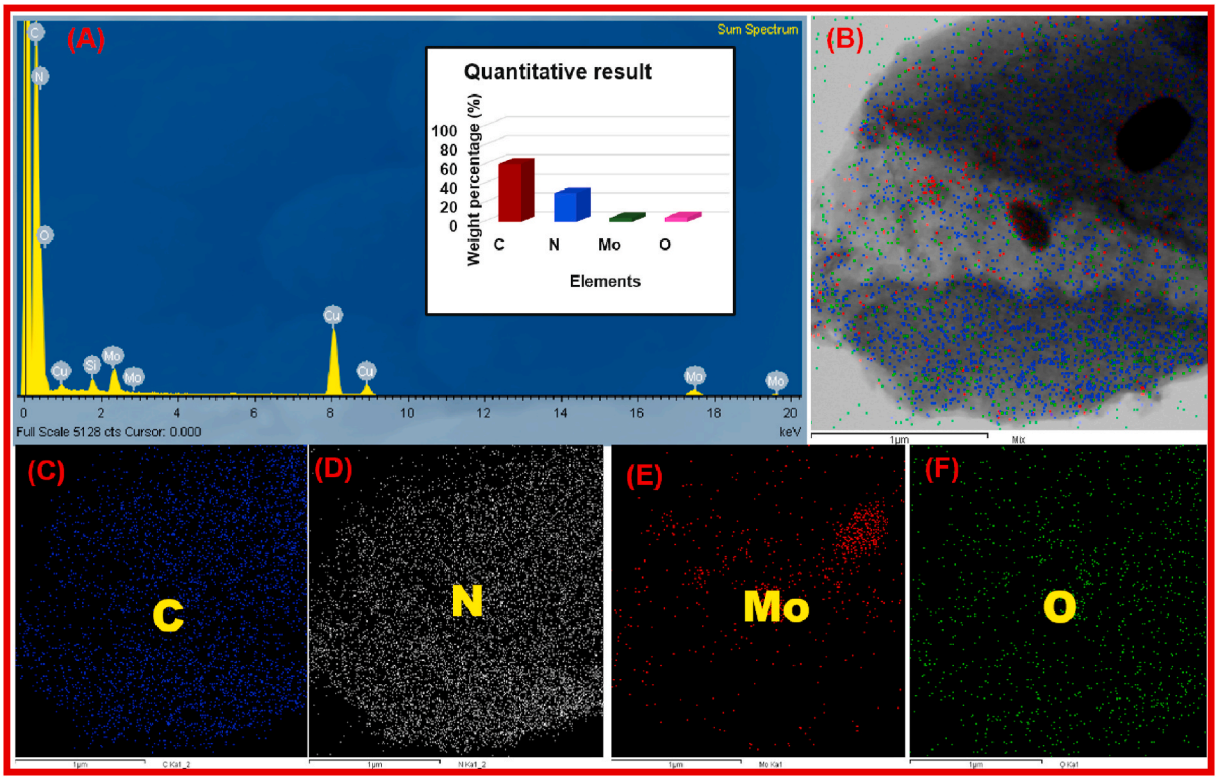

Fig. 3. (A) EDX spectrum of MoO_3@GCNS nanocomposite. Insets: Quantitative analyses. (B–F) Mapping images of MoO_3@GCNS nanocomposite individually.

$$Ip = \left(2.69\ x\ 10^5\right) n^{3/2} A C D^{1/2} v^{1/2} \quad (1)$$

The electroactive surface area of SPCE, MoO_3/SPCE, GCNS/SPCE, and MoO_3@GCNS/SPCE was found to be 0.086 cm^2, 0.137 cm^2, 0.142 $cm^{2,}$ and 0.161 cm^2 using the slope values as shown in Fig. 4C, the higher surface area of the MoO_3@GCNS modified electrode was strongly

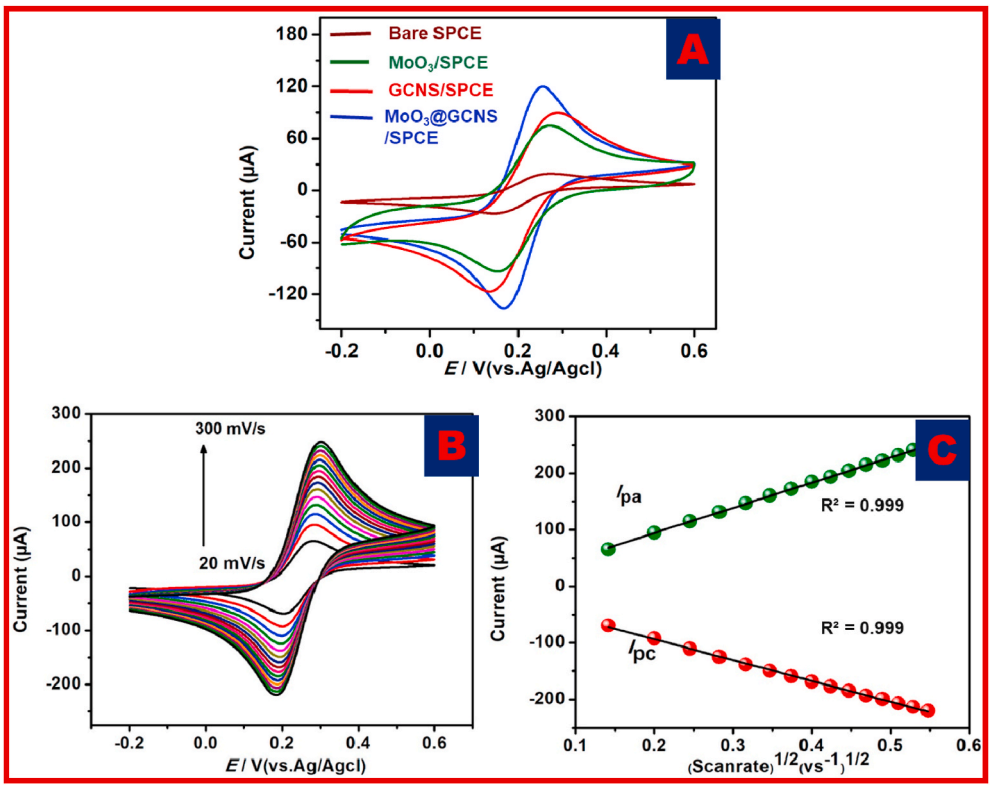

Fig. 4. CVs of SPCE, MoO_3, GCNS, and MoO_3@GCNS modified electrode in the presence of the redox probe at a sweep rate of 50 mV s^{-1} (A). CVs of MoO_3@GCNS/SPCE with the different sweep rates (20–300 mV s^{-1}) in the presence of redox probe (B). The plot of I_{pa} and I_{pc} vs. $\upsilon^{1/2}$ (C).

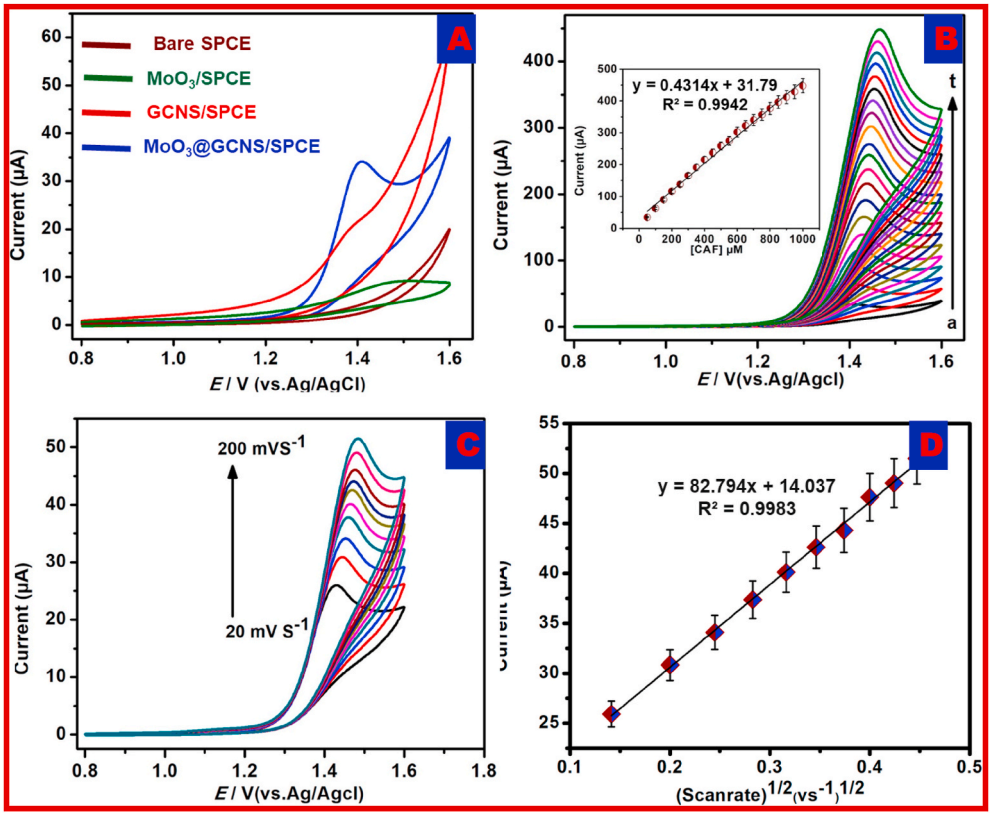

Fig. 5. CVs of 50 μM of CAF on bare SPCE, MoO_3, GCNS, and MoO_3@GCNS modified electrode in universal buffer solution at a sweep rate 50 mV s^{-1} (A). Different concentrations of CAF (50–1000 μM) at MoO_3@GCNS/SPCE (B). Insert; Calibration plot of I_{pa} vs. CAF concentration. Different scan rates (20-200 mV s^{-1}) of 50 μM CAF on MoO_3@GCNS/SPCE (C). The plot of I_{pa} vs. $\upsilon^{1/2}$ (D).

expected to increase the catalytic activity to the oxidation of CAF.

3.3. Electrocatalytic performance of MoO_3@GCNS modified electrode towards CAF

The electrochemical response of CAF at different electrodes was scrutinized in the presence of a universal buffer solution (Fig. 5A). It could be seen that the bare electrode could not display the oxidation peak current of CAF, illustrating the bare electrode has deprived electrocatalytic performance towards CAF. MoO_3 modified electrode was exhibited a small broad oxidation peak at the potential of +1.463 V and GCNS/SPCE was exhibited a noticeable oxidation signal of CAF at the potential value of +1.391 V. In contrast, MoO_3@GCNS/SPCE was exhibited sharp and precise oxidative peak potential at + 1.407 V. The oxidation peak potential was shifted towards negative potential and the I_{pa} of CAF was improved than other electrodes due to the substrate of GCNS transferred electrons through MoO_3 and enhances the electrocatalytic activity of MoO_3@GCNS towards oxidation of CAF.

The I_{pa} values of CAF were raised through the increment of CAF concentration at MoO_3@GCNS/SPCE and a linear relationship was noticed without fouling on the concentration of CAF from 50 to 1000 μM (Fig. 5B). The corresponding calibration plot is given in the insert Fig. 5B.

The electrochemical mechanism between the CAF and MoO_3@GCNS/SPCE was examined in 50 μM CAF at different sweep rates from 20 to 200 mVs^{-1} (Fig. 5C). The I_{pa} of CAF was raised with raising the sweep rate and the E_{pa} of CAF was moved positively. As can be shown in Fig. 5D, the straight-line observed for I_{pa} versus square root of scan rate and equation was expressed as I_{pa} (μA) = 82.794 $\upsilon^{1/2}$ $(Vs^{-1})^{1/2}$+ 14.037 (R^2 = 0.998) representing the electrocatalytic performance of CAF is a diffusion-controlled process at MoO_3@GCNS/SPCE, whereas the CAF molecules were diffused from the electrolyte to the surface of MoO_3@GCNS/SPCE.

3.4. DPV response for the detection CAF at MoO_3@GCNS/SPCE

DPV responses were recorded for the determination of CAF at MoO_3@GCNS/SPCE in the PB buffer solution as shown in Fig. 6A. Under the optimized experimental condition, a precise and sharp oxidation peak of CAF has been observed and the peak current increased by varying the CAF concentration (0.5 − 810 μM) as seen in Fig. 6B. At lower concentration, the I_{pa} of CAF has a linear relationship with CAF concentration proposing the detection limit (LOD) of 21.24 nM based on S/N = 3 [30].

$$LOD = 3S/q$$

Furthermore, the additional straight line was observed with increasing the concentration of CAF (410 − 810 μM) with an R^2 value of 0.993. Finally, the sensitivity was measured to be 11.584 μA μM^{-1} cm^{-2} using the lower concentration of the slope.

Moreover, the electrode material, technique, LOD, and linear response of CAF as compared with MoO_3@GCNS/SPCE are summarized in Table 1 which proposing the MoO_3@GCNS/SPCE showed wider linear range, excellent LOD, and good sensitivity for CAF sensing.

3.5. The selectivity study of MoO_3@GCNS sensor

The selectivity is an important phenomenon for electrochemical signal because of the presence of various interfering molecules affects the determination of CAF. To study the selectivity of MoO_3@GCNS modified SPCE, the potential co-interfering species such as dopamine (DA), epinephrine (Epn), folic acid (FA), acetaminophen (ACTP), uric acid (UA), tannic acid (TA), ascorbic acid (AA) and xanthine (Xan) were used in 0.1 M PB (7.0). The MoO_3@GCNS electrode shows a well-

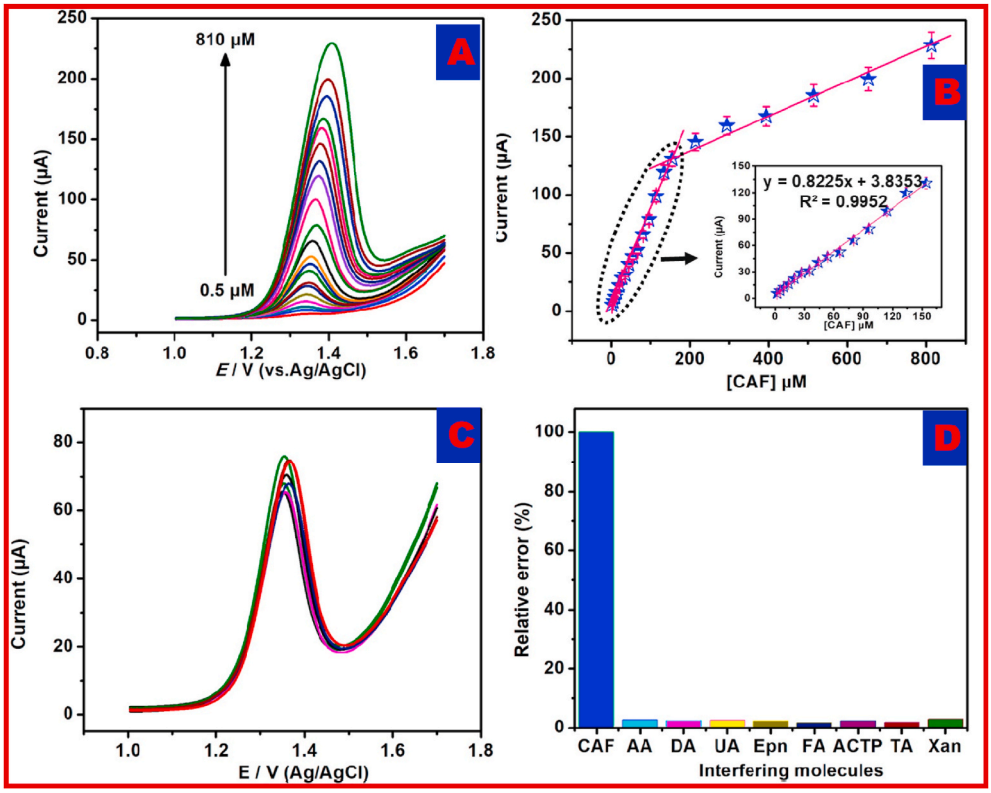

Fig. 6. DPV curves for the determination of CAF at MoO_3@GCNS/SPCE with continuous addition of CAF with various concentrations (0.5 μM–810 μM) (A). Linear response of I_{pa} vs. CAF concentration. Insert: Calibration plot for lower concentration (0.5–359 μM) (B). The DPV responses of CAF oxidation with a 20-fold concentration of interfering compounds like AA, DA, UA, Epn, FA, ACTP, TA, Xan (C). Relative error analysis for the interfering samples (D).

Table 1
The analytical parameters are compared with MoO_3@GCNS/SPCE sensor with other CAF sensors.

Electrode	LOD/ μM	Linear range/ μM	Method	Ref.
(ZnO NPs/[a]GCE)	0.038	2–100	DPV	[32]
AuNP-[b]GCPE	2.4	25–150	DPV	[33]
CeO_2-[c]SPE	2.4	5–286	DPV	[34]
[d]PLCY/[e]N-CNT/GCE	0.20	0.40–140	DPV	[35]
Cu-[f]GO-[g]CB-[h]PEDOT:PSS/ GCE	3.4	11–64	SWV	[36]
[i]EPPGE	0.008	0.02–100	SWV	[37]
$MnFe_2O_4$@N-CNT	0.51	2.9–377	SWV	[38]
MoO_3@GCNS/SPCE	0.021	0.5–810	DPV	**This work**

[a] GCE: Glassy carbon electrode.
[b] GCPE: Glassy carbon paste composite electrode.
[c] SPE: Screen printed electrode.
[d] PLCY: Poly L-Cysteine.
[e] N-CNT: Nitrogen doped carbon nNanotube.
[f] GO: Graphene oxide.
[g] CB: Carbon black.
[h] PEDOT:PSS: poly(3,4-ethylenedioxythiophene)-poly(styrenesulfonate).
[i] EPPGE: Edge plane pyrolytic graphitic electrode.

defined oxidation peak current towards 50 μM CAF, whereas the oxidation peak current of CAF was not changed in the presence of 20-fold excess of interfering species (Fig. 6C). Fig. 6D indicated the relative error (%) for the detection of CAF with a 20-fold excess of the interfering molecule. Biological compounds exhibit a 1-10% interfering effect on CAF detection. Moreover, the oxidation peak current of CAF was changed by ~4.5% in a 20-fold concentration of interfering compounds. This result was revealed the developed MoO_3@GCNS sensor has good selectivity towards CAF.

3.6. Long-term stability, reproducibility, and repeatability of the MoO_3@GCNS sensor

The long-term stability of the proposed MoO_3@GCNS/SPCE was scrutinized and kept in 0.1 M PB (7.0) at RT. The oxidation peak current of CAF was observed for every day using the same MoO_3@GCNS/SPCE. After two weeks, the current response of the MoO_3@GCNS/SPCE was retained 98.6% from its initial response indicates the MoO_3@GCNS/SPCE has good storage stability. The reproducibility of MoO_3@GCNS/SPCE investigated in 0.1 M PB (pH 7.0) containing 50 μM CAF (n = 5) and results exhibit R.S.D. value of 2.9%, which indicated that the MoO_3@GCNS sensor has good reproducibility. Repeatability of the MoO_3@GCNS/SPCE system was examined with 5 consecutive measurements of 50 μM CAF, R.S.D was calculated to be 3.2%, specifying better repeatability of the proposed sensor.

3.7. Sample analysis

Due to the higher sensitivity of MoO_3@GCNS modified electrode towards CAF detection, the amount of CAF was estimated in the green tea leaves and coffee powder extract by DPV using 0.1 M PB (7.0) (Fig. 7A and B). To prepare real samples, the 500 mg of green tea leaves and 500 mg of black coffee powder taken in the two separated beaker containing 100 mL DD water, after 10 min of stirring, the solution was boiled for 20 min at 50 °C. The required concentration of CAF was prepared using green tea and coffee powder extract instead of DD water. The added amounts and recovery outcomes were tabulated in Table 2. It was obtained that the average recoveries of CAF were 96.7% for green tea leaves and 102.8% for the coffee sample. These results suggested that the MoO_3@GCNS sensor has excellent practicability and it can be used for CAF determination in green tea leaves and coffee powder.

4. Conclusion

In summary, we successfully synthesized MoO_3@GCNS by a simple hydrothermal method. The structural and morphological characterization of synthesized nanocomposite was confirmed by XPS, FT-IR, FE-SEM, and XRD techniques. The synthesized MoO_3@GCNS modified with SPCE was studied using a redox probe by the voltammetric method. The electrocatalytic property of MoO_3@GCNS towards CAF was investigated with cost-effective disposable SPCE by differential pulse voltammetry. In this work, it was proved that MoO_3@GCNS catalyst has an excellent electrocatalytic activity to detect CAF with a lower LOD (21.24 nM), better sensitivity (11.584 μA $\mu M^{-1} cm^{-2}$), and exhibits two wide linear ranges (0.5–359 μM and 410–810 μM). Furthermore, CAF can be selectively determined in presence of interfering molecules using the

Table 2
CAF determination in green tea leaves and coffee powder using MoO_3@GCNS/SPCE

Real Samples	CAF				
	Detected/ μM	Added/ μM	Found/ μM	R.S.D. (%)	Recovery (%)
Green Tea leaves	1.37	0	1.26 ± 0.34	1.05 ± 0.23	91.9
	1.55	5	6.67 ± 0.71	2.41 ± 0.17	101.8
	2.27	10	11.84 ± 0.63	2.93 ± 1.06	96.4
Coffee powder	2.85	0	2.79 ± 1.05	1.89 ± 0.74	97.8
	3.24	5	8.57 ± 0.56	2.84 ± 1.67	104.0
	3.91	10	14.83 ± 1.31	3.20 ± 1.06	106.6

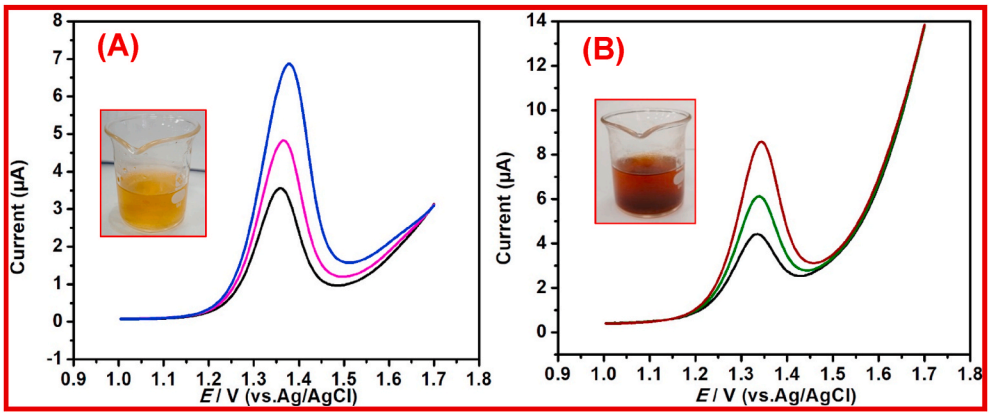

Fig. 7. DPV response for the determination of CAF at MoO_3@GCNS electrode with continuous addition of CAF with various concentrations (5,10, and 15 μM) in 0.1 M PB having green tea (pH 7.0) (A). DPV response for the determination of CAF at MoO_3@GCNS electrode with continuous addition of CAF with various concentrations (5, 10, and 15 μM) in 0.1 M PB (7.0) having coffee powder extract (pH 7.0) (B). (For interpretation of the references to colour in this figure legend, the reader is referred to the Web version of this article.)

MoO_3@GCNS/SPCE. Additionally, the practicability of the MoO_3@GCNS/SPCE was effectively demonstrated from the green tea and coffee powder samples with high accuracy.

CRediT authorship contribution statement

Gopal Boopathy: is the research student working under the. **Murugan Keerthi:** is the research scholar working under the. **S. Meenakshi:** Chen, Tawain, is corresponding authors, is corresponding authors. **M.J. Umapathy:** in Department of Chemistry, Anna University, Chennai, Associate professor, Department of chemistry, Anna University, Chennai.

Declaration of competing interest

The authors declare that they have no known competing financial interests or personal relationships that could have appeared to influence the work reported in this paper.

Acknowledgment

This project was supported by the Ministry of Science and Technology, Taiwan (ROC), (106-2113-M-027-003).

References

[1] D.A. Balentine, M.E. Harbowy, H.N. Graham, In Caffeine, CRC Press, 2019, p. 42.
[2] J.A. Nathanson, Science 226 (1984) 184.
[3] A. Nehlig, J.-L. Daval, G. Debry, Brain Res. Rev. 17 (1992) 139.
[4] S. Bolton, G. Null, Orthomol. Psychiatry 10 (1981) 202.
[5] T. Namba, T. Matsuse, Yakushigaku zasshi 37 (2002) 65.
[6] B.A. Weinberg, B.K. Bealer, The world of caffeine: the science, 2001.
[7] A.J.H. Al-naaly, Al-Qadisiyah, J. Pure Appl. Sci 19 (2017) 60.
[8] M.M. Ali, M. Eisa, M.I. Taha, B.A. Zakaria, A.A. Elbashir, Pakistan J. Nutr. 11 (2012) 336.
[9] E. Dinç, F. Onur, Anal. Chim. Acta 359 (1998) 93.
[10] Y. Zhao, C.E. Lunte, J. Chromatogr. B Biomed. Sci. Appl. 688 (1997) 265.
[11] M. Aranda, G. Morlock, J. Chromatogr. A 1131 (2006) 253.
[12] W. Xu, T.-H. Kim, D. Zhai, J.C. Er, L. Zhang, A.A. Kale, B.K. Agrawalla, Y.-K. Cho, Y.-T. Chang, Sci. Rep. 3 (2013) 2255.
[13] H. Zhang, W. Tian, L. Zhou, H. Sun, M. Tade, S. Wang, Appl. Catal. B Environ. 223 (2018) 2.
[14] Y. Sun, J. Jiang, Y. Liu, S. Wu, J. Zou, Appl. Surf. Sci. 430 (2018) 362.
[15] J. Zou, S. Wu, Y. Liu, Y. Sun, Y. Cao, J.-P. Hsu, A.T.S. Wee, J. Jiang, Carbon 130 (2018) 652.
[16] H. Zhang, W. Tian, X. Guo, L. Zhou, H. Sun, M.O. Tadé, S. Wang, ACS Appl. Mater. Interfaces 8 (2016), 35203.
[17] M. Wang, M. Shen, L. Zhang, J. Tian, X. Jin, Y. Zhou, J. Shi, Carbon 120 (2017) 23.
[18] Y. Liu, J. Jiang, Y. Sun, S. Wu, Y. Cao, W. Gong, J. Zou, RSC Adv. 7 (2017), 36015.
[19] P. Xia, B. Zhu, B. Cheng, J. Yu, J. Xu, ACS Sustain. Chem. Eng. 6 (2017) 965.
[20] L. Huang, H. Xu, R. Zhang, X. Cheng, J. Xia, Y. Xu, H. Li, Appl. Surf. Sci. 283 (2013) 25.
[21] X. Zhang, J. Yi, H. Chen, M. Mao, L. Liu, X. She, H. Ji, X. Wu, S. Yuan, H. Xu, H. Li, J. Energy Chem 29 (2019) 65–71.
[22] Y. He, L. Zhang, X. Wang, Y. Wu, H. Lin, L. Zhao, W. Weng, H. Wan, M. Fan, RSC Adv. 4 (2014), 13610.
[23] S. Patnaik, G. Swain, K. Parida, Nanoscale 10 (2018) 5950.
[24] X. Ma, Y. Lv, J. Xu, Y. Liu, R. Zhang, Y. Zhu, J. Phys. Chem. C 116 (2012), 23485.
[25] G. Liu, G. Dong, Y. Zeng, C. Wang, Chin. J. Catal. 41 (2020) 1564.
[26] Z. Xie, Y. Feng, F. Wang, D. Chen, Q. Zhang, Y. Zeng, W. Lv, G. Liu, Appl. Catal. B Environ. 229 (2018) 96.
[27] F. Qiao, J. Wang, S. Ai, L. Li, Sensor. Actuator. B Chem. 216 (2015) 418.
[28] L. Huang, F. Zhang, Y. Li, H. Wang, Q. Wang, C. Wang, H. Xu, H. Li, J. Mater. Sci. 54 (2019) 5343.
[29] C. Ma, J. Zhou, Z. Cui, Y. Wang, Z. Zou, Sol. Energy Mater. Sol. Cell. 150 (2016) 102.
[30] H. Shao, X. Zhao, Y. Wang, R. Mao, Y. Wang, M. Qiao, S. Zhao, Y. Zhu, Appl. Catal. B Environ. 218 (2017) 810.
[31] H. Yang, K. Lv, J. Zhu, Q. Li, D. Tang, W. Ho, M. Li, S.A. Carabineiro, Appl. Surf. Sci. 401 (2017) 333.
[32] R. Jagadish, S. Yellappa, M. Mahanthappa, K.B. Chandrasekhar, J. Chin. Chem. Soc. 64 (2017) 813.
[33] T. Ören, Ü. Anık, Measurement 106 (2017) 26.
[34] M. Khairy, B.G. Mahmoud, C.E. Banks, Sensor. Actuator. B Chem 259 (2018) 142.
[35] Y. Wang, Y. Ding, L. Li, P. Hu, Talanta 178 (2018) 449.
[36] A. Wong, A.M. Santos, T.A. Silva, O. Fatibello-Filho, Talanta 183 (2018) 329.
[37] R.N. Goyal, S. Bishnoi, B. Agrawal, J. Electroanal. Chem. 655 (2011) 97.
[38] D.M. Fernandes, N. Silva, C. Pereira, C. Moura, J.M. Magalhães, B. Bachiller-Baeza, I. Rodríguez-Ramos, A. Guerrero-Ruiz, C. Delerue-Matos, C. Freire, Sensor. Actuator. B Chem. 218 (2015) 128.